Decadal change in supraglacial debris cover in Baspa basin, Western Himalaya

S. Pratibha* and Anil V. Kulkarni

Divecha Centre for Climate Change, Indian Institute of Science, Bengaluru 560 012, India

Supraglacial debris cover (SDC) influences surface energy balance and glacier dynamics. However, very few studies have been carried out to understand its distribution and evolution. Previous glacier investigations carried out in Baspa basin, Western Himalaya, focus on retreat and mass balance. Therefore, the present study monitored change in SDC area from 1997 to 2014 using Landsat data. SDC area change was estimated within a 'minimum snow-free glacier area' using normalized difference snow index (NDSI) and band ratio of near infrared and shortwave infrared. Threshold values for NDSI and band ratio map were derived manually. The study was carried out for a 'minimum snow-free glacier area' of 60.5 ± 2.4 sq. km out of 174 ± 7 sq. km of total glaciated area. SDC area of 31.5 ± 1.4, 33.2 ± 1.2, 34.6 ± 1.9 and 36.3 ± 0.7 sq. km for 1997, 2000, 2011 and 2014 respectively, was estimated. Analyses show a linear increase in SDC area from 1997 to 2014 by $2.8 \pm 0.4\%$. Naradu, a benchmark glacier in the basin, show one of the highest increase in SDC area ($5.6 \pm 0.4\%$). The findings from the present study are in line with other published results that suggest retreat, glacier fragmentation and mass loss, which could be due to climate change. The present study can be extended further using the SDC map and the results, in glacier hydrology and mass balance modelling to predict future loss.

Keywords: Climate change, glaciers, remote sensing, supraglacial debris cover, western Himalaya.

Introduction

THE Himalayan glaciers are valley glaciers surrounded by steep rock walls. Weathering and erosion of these walls supply debris, which is transported down the glacier slope[1–5]. Hence, many of the glaciers in the Himalayan region are heavily debris-covered[1,2,6–9]. The supply of debris depends on temperature fluctuations, surface condition, slope and aspect of the surrounding walls[4].

The debris on the glacier surface is referred to as supraglacial debris cover (SDC). It has profound influence on the dynamics and behaviour of a glacier[10–13]. It alters the surface energy balance, as it acts as a barrier between the atmosphere and glacier ice. This in turn influences the glacier melt, as thick debris cover retards melting, and a thin layer of debris accelerates melting of underlying ice[14–18]. Studies show that SDC influences area change and retreat. Comparison of area change in clean, sparsely debris-covered and heavily debris-covered glacier showed that the latter experienced the least shrinkage and stable terminus[7,19]. However, mass loss and surface lowering has been observed in some heavily debris-covered glaciers, though the terminus was stationary[10]. Heavily debris-covered glaciers with stationary fronts have very low ice velocities as they shift the maximum glacier velocities away from the terminus[7,10,12,20]. This can result in glacier front stagnation and may lead to glacier fragmentation due to separation of the stagnant part from the main glacier body[7,21]. Thick debris cover can cause low accumulation–area ratios and influence mass balance[5,7,11,20]. Banerjee and Shankar[11] observed that specific mass balance is minimum at the terminus of a clean glacier, whereas it shifts upwards in case of debris-covered glaciers. This can result in less melting at the terminus and increased melting at higher altitudes[10,22]. Pellicciotti et al.[12] reported maximum thinning close to equilibrium line altitude (ELA) for debris-covered glaciers. Eventually, this can result in reversal of the slope and aid in the formation of supraglacial lakes[8,12,23]. It has been observed that debris-covered glaciers with lakes lose more mass than clean glaciers[8]. Melting of ice at supraglacial lakes and ice cliffs is pronounced and accounts for the large magnitude of ablation[15,20].

However, response of debris-covered glaciers to changes in climate is not uniform. Varying trends of glacial retreat and mass loss in debris-covered glaciers have been reported across different regions of the Himalaya[5,7,11,13,20,24]. Therefore, it is essential to monitor the changes in SDC to better understand the glacier dynamics, such as changes in glacier extent, hydrology and mass balance due to climate change[2,7,18].

Monitoring changes in SDC in the field is a challenge and therefore, many studies have effectively utilized remotely sensed data[2,6,25–30]. Previously developed semi-automatic approaches for mapping SDC area use multispectral data augmented by information like topography, thermal data, surface texture and geomorphometric features[2,6,18,25,27,29–32]. However, these approaches have some limitations, like they are tested on only a single
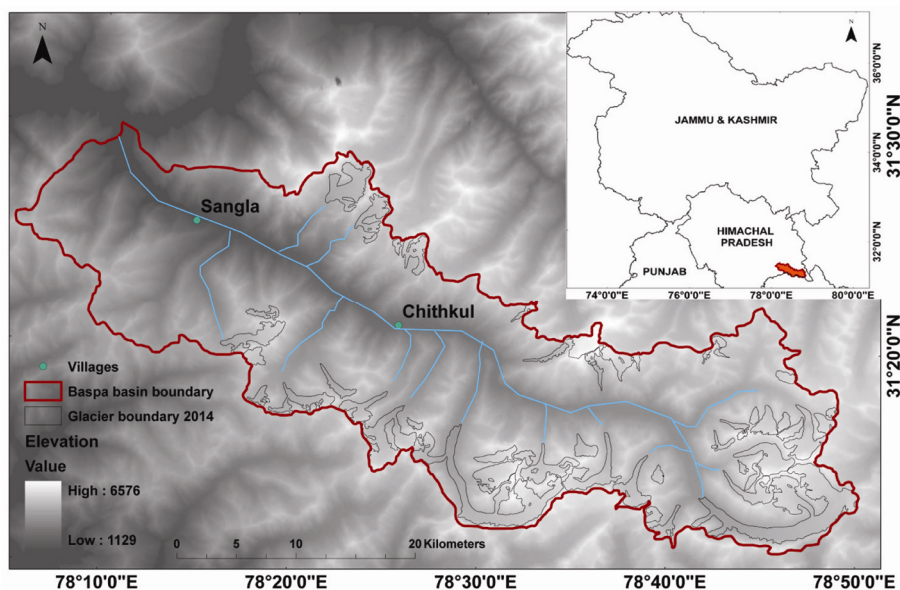
Figure 1. Location of glaciers in the study area. Baspa basin covers an area of 1050 sq. km and majority of the area is located at the elevation of 3600 masl.

Table 1. List of Landsat scenes used in the present study. The scenes fall in zone 44 of the Universal Transverse Mercator coordinate (UTM) system

Scene ID	Acquisition date
LC81460382014232LGN00	14 July 2014
LT51460382011256KHC00	7 August 2011
LE71460382001252SGS00	3 August 2001
LE71460382000218SGS00	30 June 2000
LT51460381997233ISP00	15 July 1997

glacier, use multisource data, or require specialized/coding skills or interference of specialists.

Therefore, the present study was carried out with the view of estimating the decadal change in SDC area over the entire Baspa basin, Western Himalaya, using a methodology that is computationally simple, uses freely available data and can be easily adopted in the future on a larger spatial scale than the present study area. The study uses the freely available Landsat data and glacier outlines from Randolph glacier inventory (RGI)[33] and established methods like maximum likelihood classification and band ratios[2,25,27,30,34,35].

Study area

Baspa is a sub-basin of Satluj, located in Kinnaur district, Himachal Pradesh, India (Figure 1). This high-altitude region consists of glaciers from an elevation of about 4750 to 6600 masl. The major river in the basin, Baspa, is mainly fed by snow and glacier melt run-off. The human population in the basin mainly depend on snow and glacier melt for water supply and power generation[36].

Methodology and data used

Satellite imagery

Multispectral Landsat satellite scenes of path 146 and row 38 were downloaded from http://earthexplorer.usgs.gov for the years 1997, 2000, 2001, 2011 and 2014 for ablation season (Table 1). The scenes with minimum cloud and snow were selected. Figure 2 shows the methodology followed in the present study.

Glacier boundary

We have manually modified RGI 5.0 using satellite imagery of 2014, as the glacier boundaries were of year 2000 and 2001. False colour composite (FCC) image of bands red, near infrared (NIR) and shortwave infrared (SWIR) was used for visual interpretation as ice and snow pixels stand out distinctly from surrounding classes in FCC due to their high reflectance in visible near infrared (VNIR) and low reflectance in SWIR. Also, visual cues like textures, geomorphometric features, shadow at the ice cliff, location of lateral moraines, melt run-off streams and moraine dammed lakes were considered during visual interpretation of the ablation region and snout position. The modified RGI boundary was used as the base outline for mapping SDC for all the years, thus keeping the glacier area constant throughout to quantify the percentage increase in SDC area.

Data pre-processing

The downloaded images were in the form of calibrated digital numbers (DN). As the present study uses

multisensory data, radiometric error could be induced due to difference in sensor characteristics, scene illumination, earth–sun distance, atmospheric conditions and viewing geometry. Therefore, the DNs were converted to a physically meaningful radiometric scale through radiometric correction[37]. The radiometric correction involved conversion of DN values to spectral radiance using sensor calibration parameters, which was then converted to planetary top of atmosphere (TOA) reflectance. Correction steps were adopted from Chander *et al.*[37] for thematic mapper (TM) and enhanced thematic mapper (ETM) sensors, and https://landsat.usgs.gov/Landsat8_Using_Product.php for Operational Land Imager (OLI) sensor.

Accounting for seasonal snow cover

Presence of seasonal snow cover in the ablation region causes hindrance to accurate mapping of SDC. Therefore, we have mapped the glacier area free of seasonal snow cover for all the years. Then, we combined the snow-free areas to identify the region which is free from seasonal snow for all the years. We refer to this area as 'minimum

snow-free glacier area'. Changes in SDC area were analysed within this region.

Snow-free glacier area was mapped using supervised classification of multispectral data utilizing the maximum likelihood classification (MLC) algorithm, which is based on the probability of a pixel belonging to a class. Supervised classification of VNIR and SWIR bands (0.5–1.7 μm) are used in the characterization of features of a glacier[28,30,31]. Therefore, the same band combination was used in the present study. The classification algorithm was trained using manually selected sample signatures of snow and ice pixels, and a binary image (snow and non-snow) was derived for each year. Finally, the binary images for all the years were combined in such a way that if a pixel contained snow even in a single year, it was eliminated from the minimum snow-free glacier area (Figure 3).

Accuracy assessment of the classification was carried out by randomly selecting 250 points and manually allotting the class to which the points belong. Then the error matrix was calculated to determine the user's, producer's and overall classification accuracy[38]. The average overall classification accuracy for all the years was found to be 95.8%. The change in SDC was then assessed within this minimum snow-free glacier area as described in the following section.

Mapping change in SDC area

SDC area was mapped using normalized difference snow index (NDSI) and NIR and SWIR band ratio algorithm. Glacier mapping using band ratio is based on high reflectance of ice in the visible bands and low reflectance in the SWIR band. Band ratio algorithms are fast, robust and have been already established in previous studies[2,25,29,32,34,35,39–42]. Paul *et al.*[42] compared various combinations of bands and found that the NIR and SWIR
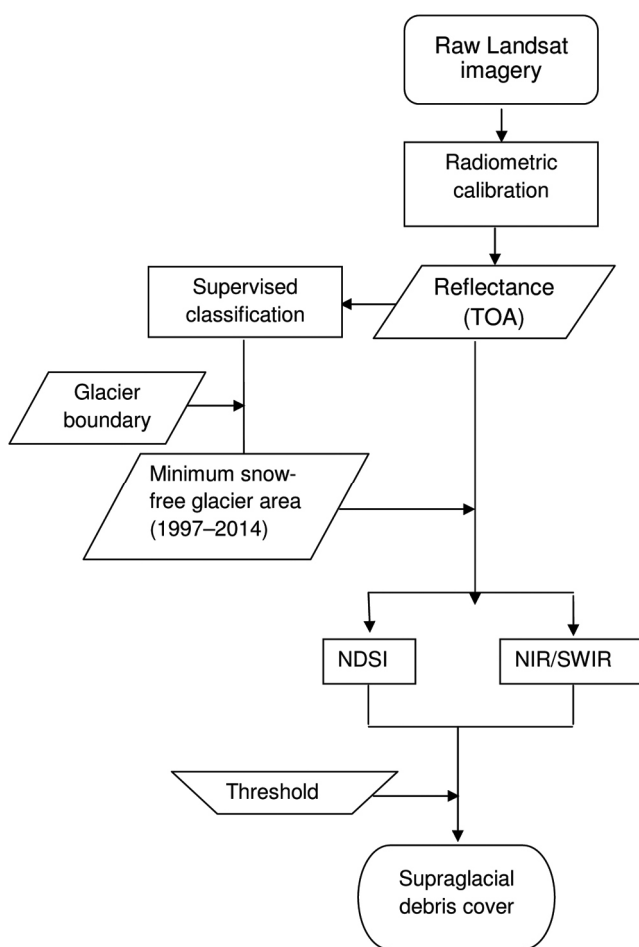
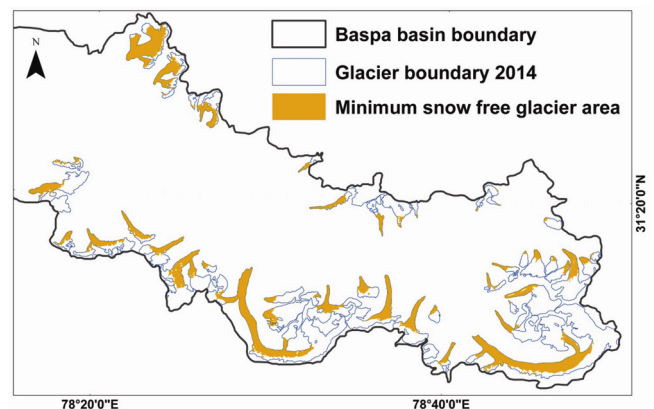**Figure 2.** Work flow for mapping SDC area within a given glacier boundary.

Figure 3. 'Minimum snow-free glacier area' for 1997, 2000, 2001, 2011 and 2014 derived by supervised classification. SDC area change analysis was carried out within this area.

ratio is best suited for glacier mapping. On the other hand, Racoviteanu *et al.*[32] found that using NDSI resulted in cleaner glacier mapping compared to other band ratios. The band ratio method is not influenced by topographic conditions and could detect snow even under mountain shadow.

NDSI is estimated as follows:

$$\text{NDSI} = \frac{\text{Green reflectance} - \text{SWIR reflectance}}{\text{Green reflectance} + \text{SWIR reflectance}}. \tag{1}$$

Finally, a threshold was applied to NDSI and NIR and SWIR ratio map to separate debris from ice. The final SDC area was derived as the average of SDC area derived from NDSI and ratio of NIR and SWIR bands. Table 2 provides the specifications of bands used in NDSI and NIR and SWIR ratio.

Determination of threshold: A plot of green reflectance as a function of NDSI shows that NDSI value around 0.2 can be used to separate debris pixels from ice pixels (Figure 4). To accurately determine an appropriate threshold, we use manually delineated SDC area of few sample glaciers. Delineation was done by visual interpretation of Landsat images. Rough texture, uneven surfaces of SDC, geomorphometric features and difference in colour compared to ice pixel aided in manual delineation. A curve was fitted in a plot of automatically derived SDC area of these sample glaciers as a function of threshold. Using this curve, an optimized threshold value was determined that produced the same area of SDC cover as the manually delineated SDC area. To avoid bias, glaciers of varying size and aspect were chosen as samples to manually delineate SDC area and the average of these thresholds was considered as the final threshold value (Table 2).

Uncertainty estimation

One of the sources of uncertainty in SDC cover mapping is the threshold value. The threshold value considered in this study is the average of those values derived manually. Therefore, the cumulative of difference in SDC area derived from the average threshold and individual threshold values was used to determine the error in SDC estimation. To determine the uncertainty in glacier boundary delineation, an error of ±4% induced due to mapping and misregistration was considered as given in the literature[3,43], based on buffer method[44].

Validation

The methodology was validated on a debris-covered glacier using ground control point (GCP) as well as on a clean glacier (Figure 5 and Table 3). Robustness of the methodology was further validated by comparing SDC of 2000 with that of 2001 in Baspa basin, as not much change is expected within a year (Table 4).

Results and discussion

The analysis was carried out on 48 glaciers covering an area of 174 ± 7 sq. km. All the glaciers in the basin were considered, whereas snow patches and snow fields were ignored. The glacier area varied from 0.3 to 31 sq. km with an average size of 3.6 sq. km. Out of the total glaciated area, 60.5 ± 2.4 sq. km was mapped as minimum snow-free glacier area. The study estimated SDC area of 31.5 ± 1.4, 33.2 ± 1.2, 34.6 ± 1.9 and 36.3 ± 0.7 sq. km respectively, for year 1997, 2000, 2011 and 2014. This shows a steady increase in SDC by $2.8 \pm 0.4\%$ from 1997 to 2014 (Figure 6 and Table 4). NDSI under-estimated SDC area compared to band ratio technique by an average of 0.16 ± 0.07 sq. km (Table 4).

Table 2. Threshold values to separate ice from debris using NDSI and NIR/SWIR band ratio

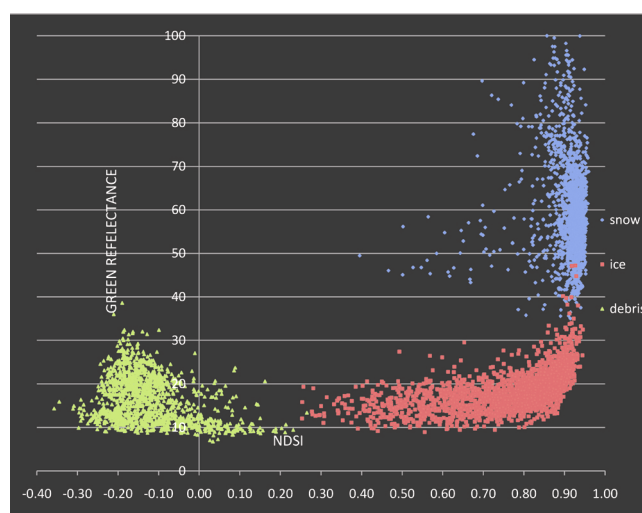| Sensor | Bands (µm) | Threshold | |
		NIR/SWIR	NDSI
OLI	(Green) band 3: 0.53–0.59 (NIR) band 5: 0.85–0.88 (SWIR) band 6: 1.57–1.65	1.54	0.222
ETM	(Green) band 3: 0.52–0.60 (NIR) band 4: 0.77–0.90 (SWIR) band 5: 1.55–1.75	1.49	0.220
TM	(Green) band 3: 0.52–0.60 (NIR) band 4: 0.76–0.90 (SWIR) band 5: 1.55–1.75	1.46	0.205

Figure 4. Plot of green reflectance as a function of normalized difference snow index (NDSI) for different classes derived from Landsat OLI imagery. Pixels corresponding to negative NDSI value belong to debris class, and a threshold value was determined to separate debris pixels from ice pixels.

Table 3. Details of glaciers and Landsat scenes used for validation

Glacier	Date	Sensor	Path/row	Basin	Glacier type
Samudra Tapu	28 June 2001	ETM	147/037	Chandra, Western Himalaya	Debris-covered
Teesta Khangtse	12 February 2001	ETM	139/41	Teesta, Eastern Himalaya	Clean

Table 4. Supraglacial debris cover area derived by ratio of NIR/SWIR and NDSI algorithm for various years

Year	NDSI SDC area (sq. km)	NIR/SWIR SDC area (sq. km)	Average SDC area (sq. km)	Average SDC area (%)
2014	36.21 ± 0.75	36.36 ± 0.68	36.28 ± 0.72	20.85 ± 0.41
2011	34.54 ± 2.0	34.66 ± 1.7	34.60 ± 1.85	19.86 ± 1.06
2001*	33.07 ± 1.28	33.25 ± 1.18	33.16 ± 1.23	19.03 ± 0.71
2000	33.12 ± 1.28	33.18 ± 1.18	33.15 ± 1.23	19.03 ± 0.71
1997	31.33 ± 1.12	31.61 ± 1.6	31.47 ± 1.36	18.06 ± 0.78

*SDC area mapped for 2001 was used for validation.
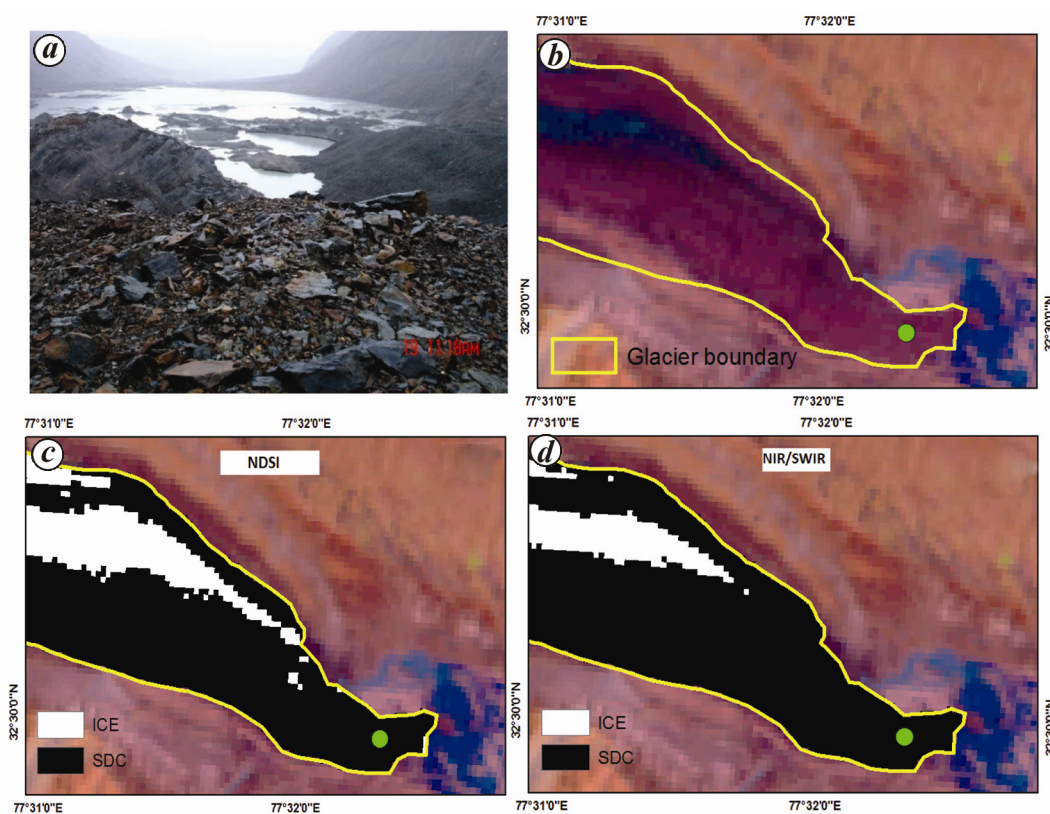

Figure 5. Validation of the study methodology on Samudra Tapu glacier. *a*, Field photograph of SDC near the terminus of Samudra Tapu glacier; *b*, FCC of bands green, red and NIR (blue, green, red) of Landsat imagery of 2001. Green dot represents the location of the GCP and the photograph; *c*, SDC area derived by NDSI; *d*, SDC area derived by ratio of NIR and SWIR.

The largest glacier in the basin, Baspa Bhamak, experienced an increase in SDC by $2.4 \pm 0.4\%$ (Figure 7). Naradu, a benchmark glacier in the basin, showed one of the highest increases in SDC by $5.6 \pm 0.4\%$ with 21% of SDC. The reason for the high increase in SDC could be the prolonged negative mass balance that Naradu glacier has experienced. Studies have shown that Naradu glacier experienced negative mass balance consistently since AD 1900 (ref. 45). Three of the glaciers showed high SDC cover; if this trend continues, they have the potential to turn into rock glaciers (Figure 7). Further, heavy SDC at glacier front can cause stagnation. This could contribute to glacier fragmentation and increase in the number of glaciers. Comparison of present glacier boundaries with that of the Geological Survey of India inventory showed glacier fragmentation in last 35 years[36].

Area–altitude distribution analysis showed that the maximum altitude of SDC was around 5600 masl and
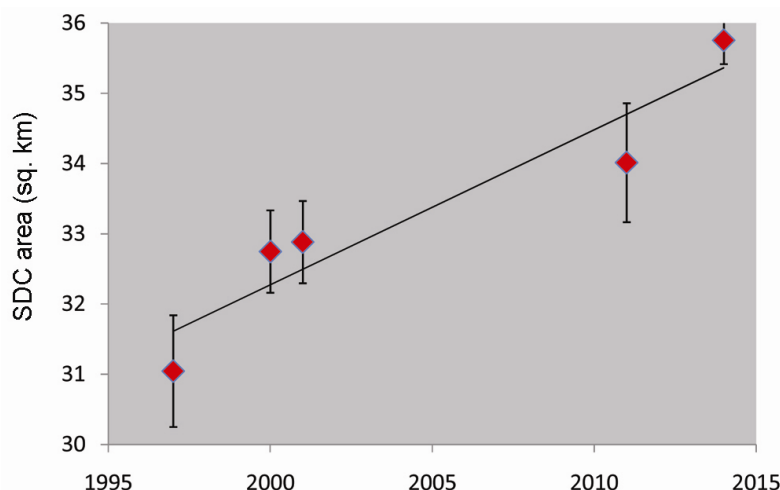
Figure 6. Graph showing increase in SDC area from 1997 to 2014. Error bar represents uncertainty in SDC area derived by thresholding NDSI and NIR/SWIR map. Highest increase in SDC for the study period observed was 7.6% for a glacier with 33% of SDC in 2014.
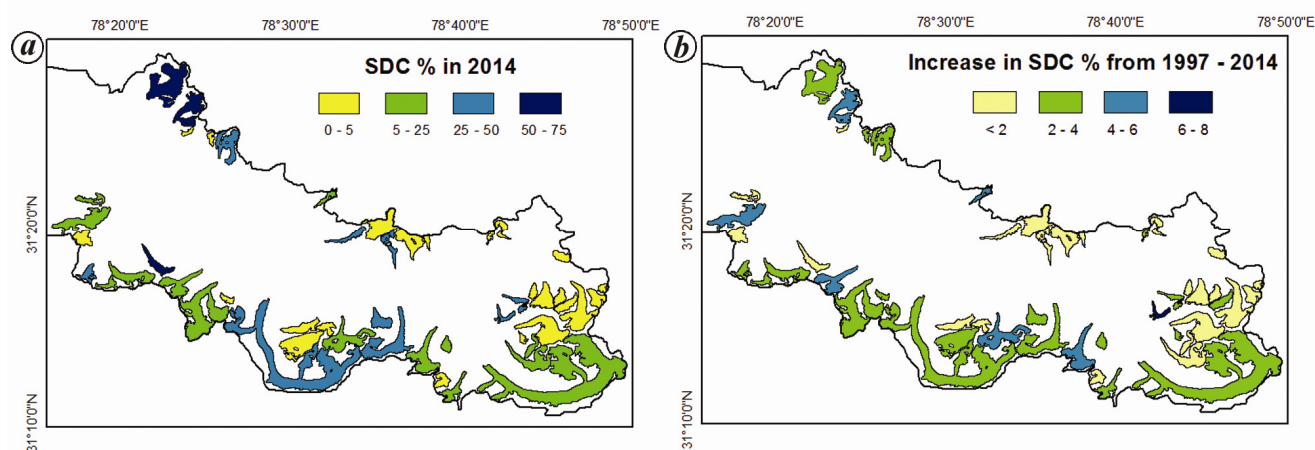

Figure 7. *a*, Percentage SDC area for 2014; *b*, Percentage increase in SDC area from 1997 to 2014. Nineteen glaciers have above average increase in SDC cover. This increase in SDC could be due to the reduction in debris-carrying capacity resulting from consistent mass loss. On the other hand, glaciers with high percentage of SDC did not show much increase. Also, the eastern part of the basin, which is at the higher altitude, consists of minimum SDC area and shows the least increase.

maximum change occurred at about 5000 masl. Clean glaciers in the basin are located at higher altitude than debris-covered glaciers. Some of these glaciers showed less SDC cover and negligible increase in SDC which are governed by the geomorphological settings.

We analysed the utility of our thresholds for deriving SDC area in other basins using manually derived SDC area for five glaciers in Landsat imagery with Scene 1d: LE71470372001179SGS. We found that the threshold value of band ratio of NIR and SWIR underestimated the SDC area by 8%, suggesting that it has the potential of mapping SDC area in the other basins with minor modifications. However, NDSI underestimated the SDC area by 23%. In addition, SDC area for 93 glaciers in the Karakorum region was derived using band ratio of NIR and

SWIR[29] and the threshold was found to be very close to that derived in the present study[31].

Conclusion

This study utilized freely available data and computationally simple approach to study decadal changes in SDC over the entire Baspa basin from 1997 to 2014. The basin consists of clean, partially debris-covered and heavily debris-covered glaciers. On an average, 20 ± 0.7% of the glaciated area is covered in SDC. More than 70% of the glaciers are partially debris-covered (<25% of SDC). The study revealed that SDC in the basin has steadily increased over the study period. Increase in SDC is

associated with consistent loss in mass and few of the glaciers showed higher increase in SDC due to prolonged negative mass balance. The findings of the present study are in line with those of previous studies on snowline, mass balance and retreat that suggest deglaciation in Baspa basin[45,46]. Heavily debris-covered glaciers are reported to have smaller accumulation area ratio and field observations in Baspa basin have reported receding or no accumulation area in a few glaciers[46]. This can be linked to increase in SDC due to inefficient debris transportation in the ablation-dominated setting. If this trend continues, these may eventually turn into rock glaciers. The present SDC map can be incorporated in the mass balance model to predict future mass loss due to climate change. This study shows that Landsat data and RGI inventory with few changes can be used for SDC study at basin-scale. The approach can be adopted at a much larger spatial scale to study the effect of climate change with respect to mass balance and increase in the number of supraglacial and moraine dammed lakes in different regions of the Himalaya.

1. Shroder, J. F., Bishop, M. P., Copland, L. and Sloan, V. F., Debris-covered glaciers and rock glaciers in the Nanga Parbat Himalaya, Pakistan. *Geogr. Ann.: Series A, Phys. Geogr.*, 2000, **82**(1), 17–31.

2. Bhambri, R., Bolch, T. and Chaujar, R. K., Mapping of debris-covered glaciers in the Garhwal Himalayas using ASTER DEMs and thermal data. *Int. J. Remote Sensing*, 2011, **32**(23), 8095–8119.

3. Racoviteanu, A. and Williams, M. W., Decision tree and texture analysis for mapping debris-covered glaciers in the Kangchenjunga area, Eastern Himalaya. *Remote Sensing*, 2012, **4**(10), 3078–3109.

4. Nagai, H., Fujita, K., Nuimura, T. and Sakai, A., Southwest-facing slopes control the formation of debris-covered glaciers in the Bhutan Himalaya. *Cryosphere*, 2013, **7**(4), 1303–1314.

5. Anderson, L. S. and Anderson, R. S., Modeling debris-covered glaciers: response to steady debris deposition. *Cryosphere*, 2016, **10**(3), 1105.

6. Bolch, T., Buchroithner, M. F., Kunert, A. and Kamp, U., Automated delineation of debris-covered glaciers based on ASTER data. In *Geoinformation in Europe*. Proceedings of the 27th EARSeL Symposium, Bolzano, Italy, 2007, pp. 4–6.

7. Scherler, D., Bookhagen, B. and Strecker, M. R., Spatially variable response of Himalayan glaciers to climate change affected by debris cover. *Nature Geosci.*, 2011, **4**(3), 156–159.

8. Basnett, S., Kulkarni, A. V. and Bolch, T., The influence of debris cover and glacial lakes on the recession of glaciers in Sikkim Himalaya, India. *J. Glaciol.*, 2013, **59**(218), 1035–1046.

9. Bhardwaj, A., Joshi, P. K., Sam, L., Singh, M. K., Singh, S. and Kumar, R., Applicability of Landsat 8 data for characterizing glacier facies and supraglacial debris. *Int. J. Appl. Earth Observ. Geoinf.*, 2015, **38**, 51–64.

10. Benn, D. I. *et al.*, Response of debris-covered glaciers in the Mount Everest region to recent warming, and implications for outburst flood hazards. *Earth-Sci. Rev.*, 2012, **114**(1), 156–174.

11. Banerjee, A. and Shankar, R., On the response of Himalayan glaciers to climate change. *J. Glaciol.*, 2013, **59**(215), 480–490.

12. Pellicciotti, F., Stephan, C., Miles, E., Herreid, S., Immerzeel, W. W. and Bolch, T., Mass-balance changes of the debris-covered glaciers in the Langtang Himal, Nepal, from 1974 to 1999. *J. Glaciol.*, 2015, **61**(226), 373–386.

13. Vincent, C. *et al.*, Reduced melt on debris-covered glaciers: investigations from Changri Nup Glacier, Nepal. *Cryosphere*, 2016, **10**(4), 1845.

14. Singh, P., Kumar, N., Ramasastri, K. S. and Singh, Y., Debris-Covered Glaciers (Proceedings of a workshop held at Seattle, Washington, USA, September 2000), IAHS Publ. No. 264, 2000.

15. Sakai, A., Takeuchi, N., Fujita, K. and Nakawo, M., *Role of Supraglacial Ponds in the Ablation Process of a Debris-covered Glacier in the Nepal Himalayas*, IAHS Publication, 2000, pp. 119–132.

16. Nicholson, L. and Benn, D. I., Calculating ice melt beneath a debris layer using meteorological data. *J. Glaciol.*, 2006, **52**(178), 463–470.

17. Zhang, Y., Fujita, K., Liu, S., Liu, Q. and Nuimura, T., Distribution of debris thickness and its effect on ice melt at Hailuogou glacier, southeastern Tibetan Plateau, using *in situ* surveys and ASTER imagery. *J. Glaciol.*, 2011, **57**(206), 1147–1157.

18. Pratap, B., Dobhal, D. P., Mehta, M. and Bhambri, R., Influence of debris cover and altitude on glacier surface melting: a case study on Dokriani Glacier, central Himalaya, India. *Ann. Glaciol.*, 2015, **56**(70), 9–16.

19. Ali, I., Shukla, A. and Romshoo, S. A., Assessing linkages between spatial facies changes and dimensional variations of glaciers in the upper Indus Basin, western Himalaya. *Geomorphology*, 2017, **284**, 115–129.

20. Thompson, S., Benn, D. I., Mertes, J. and Luckman, A., Stagnation and mass loss on a Himalayan debris-covered glacier: processes, patterns and rates. *J. Glaciol.*, 2016, **62**(233), 467–485.

21. Kulkarni, A. V., Bahuguna, I. M., Rathore, B. P., Singh, S. K., Randhawa, S. S., Sood, R. K. and Dhar, S., Glacial retreat in Himalaya using Indian Remote Sensing satellite data. *Curr. Sci.*, 2007, **92**(1), 69–74.

22. Dobhal, D. P., Mehta, M. and Srivastava, D., Influence of debris cover on terminus retreat and mass changes of Chorabari Glacier, Garhwal region, central Himalaya, India. *J. Glaciol.*, 2013, **59**(217), 961–971.

23. Reynolds, J. M., *On the Formation of Supraglacial Lakes on Debris-covered Glaciers*. In Proceedings of a Workshop held at Seattle, Washington, USA, September 2000, IAHS Publication No. 264, 2000, pp. 153–164.

24. Kääb, A., Berthier, E., Nuth, C., Gardelle, J. and Arnaud, Y., Contrasting patterns of early twenty-first-century glacier mass change in the Himalayas. *Nature*, 2012, **488**(7412), 495–498.

25. Paul, F., Huggel, C. and Kääb, A., Combining satellite multispectral image data and a digital elevation model for mapping debris-covered glaciers. *Remote Sensing Environ.*, 2004, **89**(4), 510–518.

26. Ranzi, R., Grossi, G., Iacovelli, L. and Taschner, S., Use of multispectral ASTER images for mapping debris-covered glaciers within the GLIMS project. In Proceedings of the IEEE International, Geoscience and Remote Sensing Symposium, Anchorage, AK, USA, IGARSS'04, 2004, vol. 2, pp. 1144–1147.

27. Shukla, A., Gupta, R. and Arora, M. K., Delineation of debris-covered glacier boundaries using optical and thermal remote sensing data. *Remote Sensing Lett.*, 2010, **1**(1), 11–17.

28. Khan, A., Naz, B. S. and Bowling, L. C., Separating snow, clean and debris-covered ice in the Upper Indus Basin, Hindukush–Karakoram–Himalayas, using Landsat images between 1998 and 2002. *J. Hydrol.*, 2015, **521**, 46–64.

29. Herreid, S., Pellicciotti, F., Ayala, A., Chesnokova, A., Kienholz, C., Shea, J. and Shrestha, A., Satellite observations show no net change in the percentage of supraglacial debris-covered area in northern Pakistan from 1977 to 2014. *J. Glaciol.*, 2015, **61**(227), 524–536.

30. Shukla, A., Gupta, R. P. and Arora, M. K., Estimation of debris cover and its temporal variation using optical satellite sensor data:

a case study in Chenab basin, Himalaya. *J. Glaciol.*, 2009, **55**(191), 444–452.

31. Karimi, N., Farokhnia, A., Karimi, L., Eftekhari, M. and Ghalkhani, H., Combining optical and thermal remote sensing data for mapping debris-covered glaciers (Alamkouh Glaciers, Iran). *Cold Reg. Sci. Technol.*, 2012, **71**, 73–83.

32. Racoviteanu, A., Arnaud, Y., Williams, M. W. and Manley, W. F., Spatial patterns in glacier characteristics and area changes from 1962 to 2006 in the Kanchenjunga–Sikkim area, eastern Himalaya. *Cryosphere*, 2014, **9**, 505–523.

33. Pfeffer, W. T. *et al.*, The Randolph glacier inventory: a globally complete inventory of glaciers. *J. Glaciol.*, 2014, **60**(221), 537–552.

34. Svoboda, F. and Paul, F., A new glacier inventory on southern Baffin Island, Canada, from ASTER data: I. Applied methods, challenges and solutions. *Ann. Glaciol.*, 2009, **50**(53), 11–21.

35. Hall, D. K., Ormsby, J. P., Bindschadler, R. A. and Siddalingaiah, H., Characterization of snow and ice reflectance zones on glaciers using Landsat Thematic Mapper data. *Ann. Glaciol.*, 1987, **9**(1), 104–108.

36. Kulkarni, A. V. and Alex, S., Estimation of recent glacial variations in Baspa Basin using remote sensing technique. *J. Indian Soc. Remote Sensing*, 2003, **31**(2), 81–90.

37. Chander, G., Markham, B. L. and Helder, D. L., Summary of current radiometric calibration coefficients for Landsat MSS, TM, ETM+, and EO-1 ALI sensors. *Remote Sensing Environ.*, 2009, **113**(5), 893–903.

38. Congalton, R. G., A review of assessing the accuracy of classifications of remotely sensed data. *Remote Sensing Environ.*, 1991, **37**(1), 35–46.

39. Dozier, J., Spectral signature of alpine snow cover from the Landsat Thematic Mapper. *Remote Sensing Environ.*, 1989, **28**, 9–22.

40. Hall, D. K., Riggs, G. A. and Salomonson, V. V., Development of methods for mapping global snow cover using moderate resolution imaging spectroradiometer data. *Remote Sensing Environ.*, 1995, **54**(2), 127–140.

41. Kulkarni, A. V., Srinivasulu, J. and Manjul, S. S., Field based spectral reflectance studies to develop NDSI method for snow cover monitoring. *J. Indian Soc. Remote Sensing*, 2002, **30**(1), 73–80.

42. Paul, F., Kääb, A., Maisch, M., Kellenberger, T. and Haeberli, W., The new remote-sensing-derived Swiss glacier inventory: I. methods. *Ann. Glaciol.*, 2002, **34**(1), 355–361.

43. Bhambri, R., Bolch, T., Chaujar, R. K. and Kulshreshtha, S. C., Glacier changes in the Garhwal Himalaya, India, from 1968 to 2006 based on remote sensing. *J. Glaciol.*, 2011, **57**(203), 543–556.

44. Bolch, T., Menounos, B. and Wheate, R., Landsat-based inventory of glaciers in western Canada, 1985–2005. *Remote Sensing Environ.*, 2010, **114**(1), 127–137.

45. Kumar, G. V., Kulkarni, A. V., Gupta, A. K. and Sharma, P., Mass balance estimation using geodetic method for glaciers in Baspa basin, Western Himalaya. *Curr. Sci.*, 2017, **113**(3), 486–492.

46. Kulkarni, A. V., Rathore, B. P. and Alex, S., Monitoring of glacial mass balance in the Baspa basin using accumulation area ratio method. *Curr. Sci.*, 2004, **86**(1), 185–190.